ADVANCED ENERGY MATERIALS
www.advenergymat.de

Autonomous Optimization of Air-Processed Perovskite Solar Cell in a Multidimensional Parameter Space

Jiyun Zhang, Vincent M. Le Corre, Jianchang Wu, Tian Du, Tobias Osterrieder, Kaicheng Zhang, Handan Zhang, Larry Lüer, Jens Hauch, and Christoph J. Brabec**

Traditional optimization methods often face challenges in exploring complex process parameter spaces, which typically result in suboptimal local maxima. Here an autonomous framework driven by a machine learning (ML)-guided automated platform is introduced to optimize the fabrication conditions of additive- and passivation-free perovskite solar cells (PSCs) under ambient conditions. By effectively exploring a 6D parameter space, this method identifies five parameter sets achieving efficiencies above 23%, with a peak efficiency of 23.7% with limited experimental budgets. Feature importance analysis indicates that the rotation speeds during the first and second steps of perovskite processing are the most influential factors affecting device performance, thereby meriting prioritization in the optimization efforts. These results demonstrate the exceptional capability of the autonomous framework in addressing complex process parameter optimization challenges and its potential to advance perovskite photovoltaic technology. Beyond PSCs, this work provides a reliable and comprehensive strategy for optimizing solution-processed semiconductors and highlights the broader applications of autonomous methodologies in materials science.

1. Introduction

Over recent decades, metal-halide perovskite solar cells (PSCs) have emerged as a groundbreaking technology in the renewable energy field due to their remarkable efficiency improvements.[1–3] So far, the preparation of high-performance perovskite devices typically necessitates inert atmospheres (e.g., nitrogen gloveboxes), dramatically increasing production costs and complexity, thereby hindering scalability.[4,5] Therefore, manufacturing perovskite devices in ambient air is a viable alternative to circumvent these limitations.[6–9] Developing a dependable air-processed procedure for fabricating solution-processed PSCs often requires carefully optimizing process parameters within a high-dimensional parameter space.[10–12] However, simultaneously optimizing these parameters is inherently challenging due to the complex intercorrelations among variables.[13] Traditional Edisonian methods proved inadequate in this context because of their inherent rigidity and inability to effectively untangle complex, nonlinear interdependencies among the parameters.[14,15] Moreover, these conventional approaches typically rely on linear and single-variable optimization processes that are susceptible to suboptimal local maxima, thus limiting their ability to uncover global solutions.[16] Consequently, advanced techniques capable of reproducing laboratory work and intelligently preselecting experimental conditions are highly required for streamlining and expediting optimization tasks.

Automated acceleration platforms, known as materials' acceleration platforms (MAPs) and device acceleration platforms (DAPs), have emerged as transformative tools in materials science.[17–25] These platforms enable accelerated discoveries and unparalleled efficiency gains through rapid preparation and systematic exploration.[26–29] The methodology of utilizing automation in functional energy materials' research, especially for perovskite-based materials, is drawing growing attention.[30–33] In perovskite photovoltaics, automated fabrication systems have introduced a paradigm shift by minimizing operator-induced variability and enhancing the consistency of device properties.[34,35] Despite these advantages, a significant limitation of current automated platforms is their inability to adapt and make intelligent decisions, a capability crucial for optimizing parameter sets in complex high-dimensional spaces.

J. Zhang, V. M. Le Corre, J. Wu, T. Du, T. Osterrieder, J. Hauch, C. J. Brabec
Forschungszentrum Jülich GmbH
Helmholtz-Institute Erlangen-Nürnberg (HI ERN)
High Throughput Methods in Photovoltaics
Immerwahrstraße 2, 91058 Erlangen, Germany
E-mail: jiyun.zhang@fau.de; christoph.brabec@fau.de
J. Zhang, V. M. Le Corre, J. Wu, K. Zhang, H. Zhang, L. Lüer, J. Hauch, C. J. Brabec
Friedrich-Alexander-University Erlangen-Nuremberg (FAU)
Faculty of Engineering
Department of Material Science
Institute of Materials for Electronics and Energy Technology (i-MEET)
Martensstrasse 7, 91058 Erlangen, Germany

The ORCID identification number(s) for the author(s) of this article can be found under https://doi.org/10.1002/aenm.202404957

DOI: 10.1002/aenm.202404957

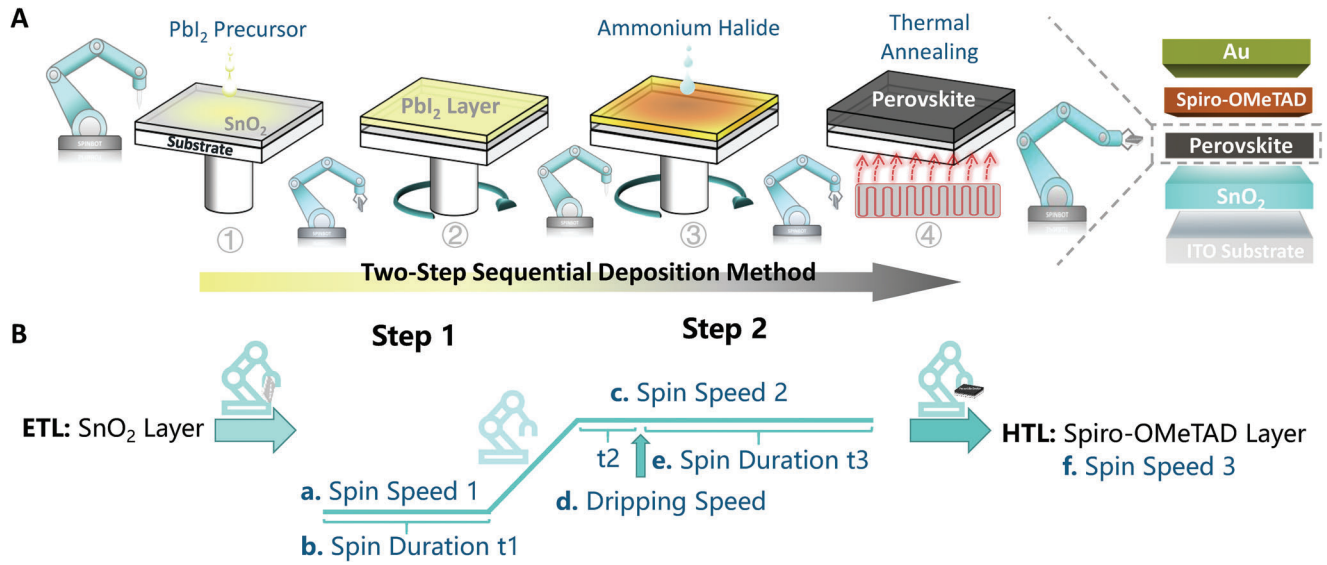

Figure 1. Schematic of the fabrication process for full perovskite devices in the air. A) Schematic of the automated preparation for PSCs with an n–i–p structure (ITO/SnO_2/perovskite/Spiro-OMeTAD/Au) using the two-step sequential deposition method. B) Pipeline diagram of the automated preparation procedure for full PSCs and the six process parameters (*a–f*) selected for global optimization.

To maximize efficiency, integrating machine learning (ML) algorithms, such as Bayesian optimization (BO), into automated platforms has emerged as a powerful strategy for optimizing material exploration.[10,36–40] These autonomous methodologies intelligently leverage real-time experimental feedback to guide automation, deciphering patterns and trends within complex datasets. By systematically exploring the intricate interdependencies among highly correlated parameters, these intelligent systems efficiently identify optimal conditions.[41,42] Such integrated self-driving platforms significantly accelerate convergence toward the most effective device configurations.[43] This autonomous approach holds huge promise for unlocking the full potential of perovskite-based devices and advancing renewable energy technologies.

In this study, we empowered an automated device acceleration platform, SPINBOT (Figure S1, Supporting Information), with an ML algorithm to optimize the process parameters for fabricating full perovskite devices under ambient conditions. The autonomous framework demonstrated its effectiveness by exploring a 6D parameter space to maximize device efficiency. With only 77 trials of process parameter sets, this framework successfully identified several parameter combinations that delivered device efficiencies exceeding 23%, with a peak efficiency of 23.7%. These results contribute to advancement in perovskite photovoltaic technology and highlight the transformative potential of intelligent, autonomous optimization methodologies in materials science.

2. Results and Discussion

2.1. Automated Fabrication of Perovskite Solar Cells in Ambient Air

Figure 1A illustrates the automated fabrication process for the perovskite layer in a metal-halide perovskite device with an n–i–p structure of ITO/SnO_2/perovskite/Spiro-OMeTAD/Au (ITO: indium tin oxide). The thin films are fabricated using a two-step sequential deposition method under ambient conditions. Specifically, the process begins with the deposition of a PbI_2 precursor onto a SnO_2-coated ITO substrate to form a wet PbI_2 layer without thermal annealing. This is followed by dripping an organic ammonium halide solution (FAI/MACl) onto the wet film, which is subsequently annealed to form the perovskite layer. As depicted in Figure 1B, the pipeline schematic outlines the automated platform's sequential execution of the solution-processed deposition steps, including the active and transport layers. The complete fabrication workflow is demonstrated in Video S1 (Supporting Information).

The preparation of stacked perovskite devices involves many process parameters, each with the potential to significantly influence overall device performance. To gain deeper insights into these effects, we compiled a comprehensive list of process parameters, as shown in Figure S2 (Supporting Information). In a previous study, we used the one-variable-at-a-time (OVAT) approach to study these parameters individually, which allowed us to identify those most critical to device performance.[44] By systematically varying a single parameter while keeping all others constant, the OVAT method effectively isolates and highlights the specific impact of each variable on device performance.

Building on this foundation, we identified six key process parameters (labeled as parameters *a–f* in Figure 1B) for global optimization to enhance the overall performance of the devices. These parameters include spin-coating speeds and durations at various fabrication stages, the dripping speed of the ammonium halide precursor, and others, as detailed in **Table 1**. The SPINBOT platform significantly surpasses manual fabrication methods by generating high-quality datasets and providing precise control over traditional unregulated parameters, such as the tip height and ejection speed of the dripping nozzle, with fine granularity

Table 1. Six input process variables and their respective optimization ranges.

Process variable	Design range	Interval	Process variable	Design range	Interval
a. Spin speed 1	500–3000 rpm	10 rpm	*d*. Dripping speed	10–500 µL s^{-1}	5 µL s^{-1}
b. Spin duration, t_1	5–50 s	1 s	*e*. Spin duration, t_3	5–45 s	1 s
c. Spin speed 2	500–3000 rpm	10 rpm	*f*. Spin speed 3	1000–5000 rpm	10 rpm

(e.g., increments of 1 rpm, 0.1 mm, 0.1 µL s^{-1}), as shown in Figure S3 (Supporting Information).[11,45] This advanced capability not only improves data integrity but also broadens the optimization scope by introducing additional parameter dimensions into the process. The ability of the automation platform to precisely control these parameters enables the construction of a 6D parameter space. This holistic and comprehensive exploration minimizes the risk of overlooking potential combinations for optimal device performance. Importantly, this automated platform is designed to optimize parameters within practical and experimental meaningful intervals rather than being restricted to minimal changes. This ensures that selected parameter settings are impactful and well suited to specific experimental conditions.

2.2. Workflow of the Autonomous Closed-Loop Optimization Method

Figure 2 presents the schematic of the autonomous iterative optimization process for high-performance perovskite devices, articulated into four interconnected stages. The process begins with the identification of key process parameters that significantly influence device performance using the OVAT method. This approach evaluates the relationship between each independent variable and the output performance. By isolating critical parameters and excluding nonessential ones, this approach simplifies the optimization process and reduces experimental costs. Building on this foundation, a multidimensional parameter space is constructed, enabling a transition from single-variable optimization to a more comprehensive and integrated analysis. To effectively sample this parameter space, the Latin hypercube sampling (LHS) method is used to determine 32 initial representative parameter sets (as detailed in Table S1 in the Supporting Information). Unlike simple random sampling, the LHS method ensures more uniform and systematic coverage of the design space, effectively minimizing the number of iterative rounds required in the subsequent optimization stages.[43] The generated parameter sets serve as the starting points for subsequent iterative experiments. Devices are fabricated using the SPINBOT platform, which ensures precise control of standard operating procedures to maintain consistency and reproducibility throughout the experiment process. After fabrication, the performance of each device is evaluated through *J*–*V* characterization, with a primary

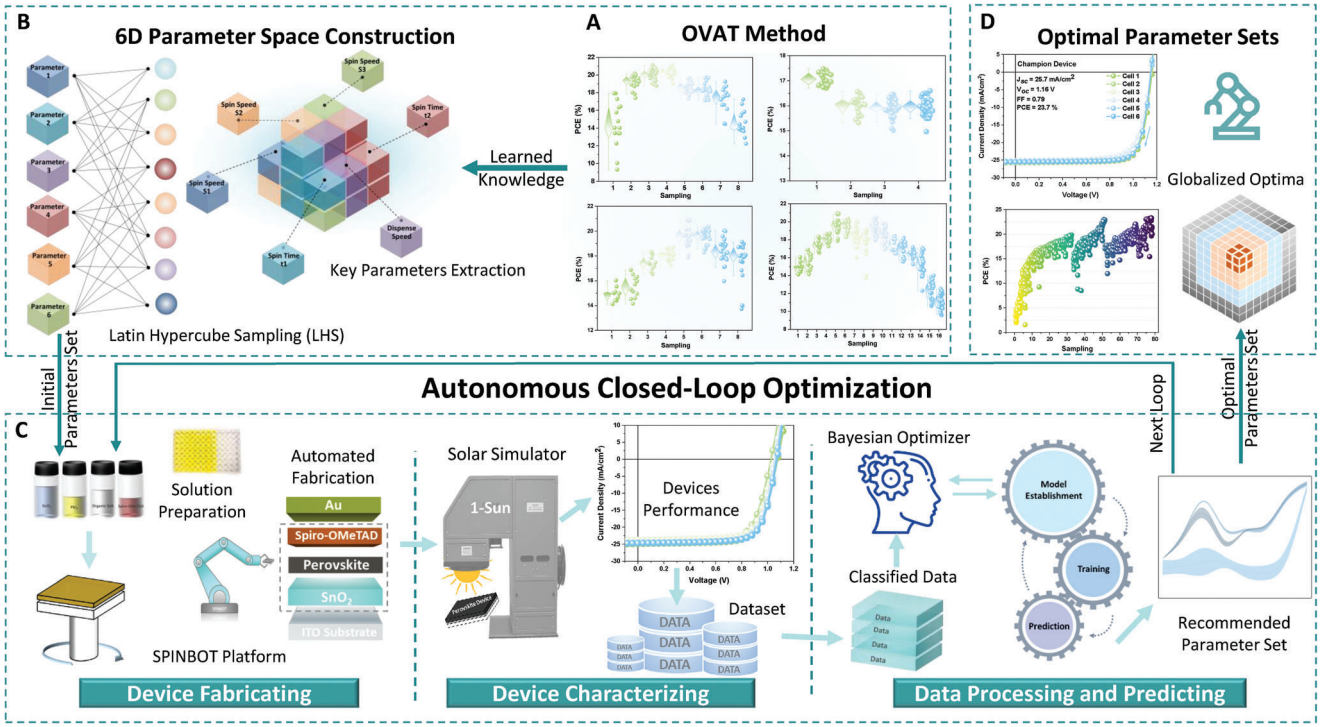

Figure 2. Schematic of the autonomous optimization workflow for high-performance air-processed perovskite devices. A) Identification of key process parameters using the OVAT method. B) Construction of a 6D parameter space and selection of initial parameter sets through the Latin hypercube sampling method. C) Execution of ML-driven autonomous iterative experimentation to maximize device efficiency, including device fabrication, characterization, data processing, and prediction of parameter sets for subsequent iterations. D) Final attainment of optimized parameter sets for device fabrication.

focus on efficiency metrics such as power conversion efficiency (PCE), fill factor (FF), open-circuit voltage (V_{oc}), and short-circuit current (J_{sc}), as shown in Figure S4 (Supporting Information). The resulting dataset is categorized and fed into the BO model to guide the next round of experiments. This iterative process refines the model's understanding of the relationship between process parameters and device performance.

The BO model was implemented using our home-developed open-source BO package BOAR.[46–48] BOAR integrates a simplified common interface for BO procedures from scikit-optimize and Ax/BOTorch frameworks,[49–51] complemented by custom utilities for analyzing solar energy material data and modeling. In this work, the "fully-Bayesian" procedure from Ax was used. This procedure enables a more accurate surrogate model thanks to the BO with sparse axis-aligned subspace method.[52,53] This procedure has been shown to provide a better fitting of the surrogate model thanks to improved hyperparameter tuning, leading to more robust optimization results. A Gaussian process regression (GPR) model with a Matern kernel was chosen as the surrogate function, and expected improvement (EI) was used as the acquisition function. At each iteration, the acquisition function predicted the parameter sets with the highest expected gain, enhancing the efficiency of the optimization process. The BO model systematically processed and analyzed the obtained data to predict the performance of unexplored parameter combinations. Armed with these predictions, the model then strategically selected new parameter combinations for experimental validation in subsequent iterations. Through multiple iterations, this systematical optimization process incrementally narrowed down the parameter space and ultimately converged on the most optimal conditions to maximize the efficiency of the perovskite device.

2.3. Autonomous Optimization Experimentation

The density plots of 2D partial dependence in **Figure 3** visually depict the multidimensional parameter space exploration conducted using the BO model. These plots illustrate the model's sampling concentration across the parameter pairs and reveal regions where more iterations were allocated. Such focused exploration highlights potential synergies between parameters that could enhance device performance. Histograms along the diagonal of the matrix show the distribution of sampled values for each parameter. Peaks in these histograms indicate higher sampling frequencies, suggesting areas where the model predicts a higher likelihood of achieving optimal outcomes. Together, the density plots and histograms showcase the algorithm's capability to intelligently navigate the multidimensional space, iteratively refining its search based on performance feedback to identify the most promising regions for enhancing device efficiency.

Figure 4 presents the influence of various process parameters on device performance. The bar charts qualitatively depict the relative importance of process parameters, referred to as "feature importance," derived from the statistical analysis of data point dispersion. Higher feature importance values indicate a relatively greater impact on performance. In Figure 4A, the feature importance of the process parameters on PCE is presented. Among the evaluated parameters, the initial spin speed (spin speed 1) has the most significant impact on PCE. Other parameters, such as the spin speed during the second step (spin speed 2) and the dripping speed of the organic ammonium halide solution (dripping speed), also show high feature importance, with values close to 0.8 and slightly below 0.5, respectively. These findings emphasize their crucial roles in fine-tuning device efficiency. Conversely, the duration of the initial spin (spin duration, t_1) and the spin speed during the HTL deposition (spin speed 3) exhibit lesser impacts, while the duration after solution dripping (spin duration, t_3) has minimal influence, with a feature importance value below 0.2. For FF, as shown in Figure 4B, spin speed 1 remains the most influential parameter, underscoring its critical role in optimizing the device FF. For J_{sc} (Figure S5, Supporting Information), spin speed 2 emerges as the most impactful parameter, closely followed by spin speed 1. Regarding V_{oc}, as shown in Figure S6 (Supporting Information), the feature importance ranking mirrors that for PCE, although the variations between parameters are less pronounced.

The feature importance of spin speed 1 for V_{oc} and FF is understandable, as this parameter directly impacts the thickness of the PbI_2 layer and the amount of residual solvent, both of which are crucial for the subsequent reaction with FAI.[54] These factors play a significant role in determining the crystallization process and, consequently, the overall quality of the perovskite film. However, the complexity of the parameter space introduces challenges that cannot be fully understood or optimized without deeper insights into the underlying mechanisms. The BO model addresses this limitation effectively by functioning as a "black box," which analyzes input and output data without relying on specific mechanistic assumptions.[28,37,55]

To better visualize the influence of process parameters on device performance, correlation analysis between these parameters and performance metrics was performed using scatter plots and trend lines. Figure 4C and Figure S7 (Supporting Information) show the relationship between PCE and individual processing parameters. This relationship was modeled using a GPR surrogate projected into 1D to analyze the influence of a single parameter while maintaining optimal conditions for the others. PCE exhibits a nonlinear relationship with spin speed 1, where an optimal speed (e.g., 1500 rpm) maximizes PCE before it declines at higher speeds. Spin speed 2 shows a more complex nonlinear trend, increasing efficiency to a certain threshold before leveling off. In contrast, spin duration t_1 demonstrates a weak correlation with efficiency, with shorter spin times (e.g., 15–20 s) proving more favorable. The relationship between dripping speed and PCE highlights stabilization at relatively higher speeds (e.g., 250 $\mu L\ s^{-1}$) after fluctuations at lower speeds. This trend diverges from observations made using the OVAT method,[44] highlighting the limitations of OVAT in capturing the multifaceted interactions within the parameter space. These findings emphasize the intricate interplay between parameters, where optimal values are often nonintuitive and influenced by interactions with other variables. Such complexity validates the advantages of employing an autonomous approach for global optimization.

Figure 4D presents the relationship between FF and spin speeds during perovskite processing, revealing nonlinear correlations. For spin speed 1, a distinct peak is observed

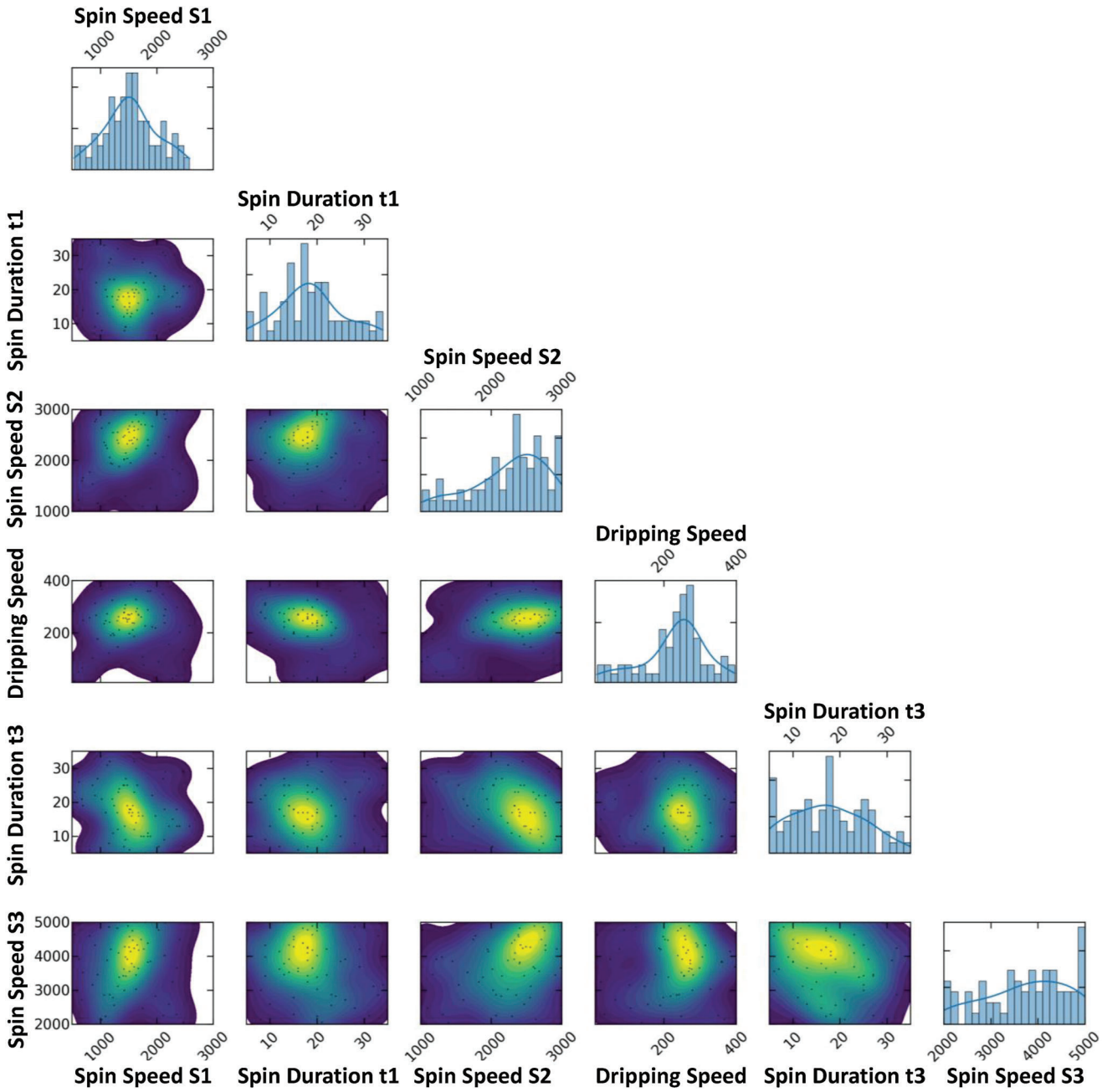

Figure 3. Interactive density plots of 2D partial dependence during parameter space exploration using the autonomous framework.

where FF is maximized at a specific speed. For spin speed 2, FF initially increases with higher speeds but then gradually decreases, although the decline is less pronounced than the sharp peak observed for spin speed 1. Figures S8–S10 (Supporting Information) further detail the relationship between process parameters, and the FF, V_{oc}, and J_{sc} metrics of perovskite devices, respectively. The trends of V_{oc} closely mirror those of PCE, with significant fluctuations in response to parameter changes. The wide spread of data points indicates that V_{oc} is highly sensitive to these parameters, where even minor adjustments can lead to substantial variations. Conversely, the influence of process parameters on J_{sc} is minimal, with flat trends and only slight fluctuations being observed across a broad range of settings. These results collectively underscore the critical importance of prioritizing speed parameters during the spin-coating process to optimize device performance. Precise control of spin speeds is essential for achieving high-quality perovskite films. Additionally, the precursor dispensing speed and the initial spin duration emerge as pivotal control parameters. This further highlights the necessity for precise control of these fabrication steps to maximize the performance of PSCs.

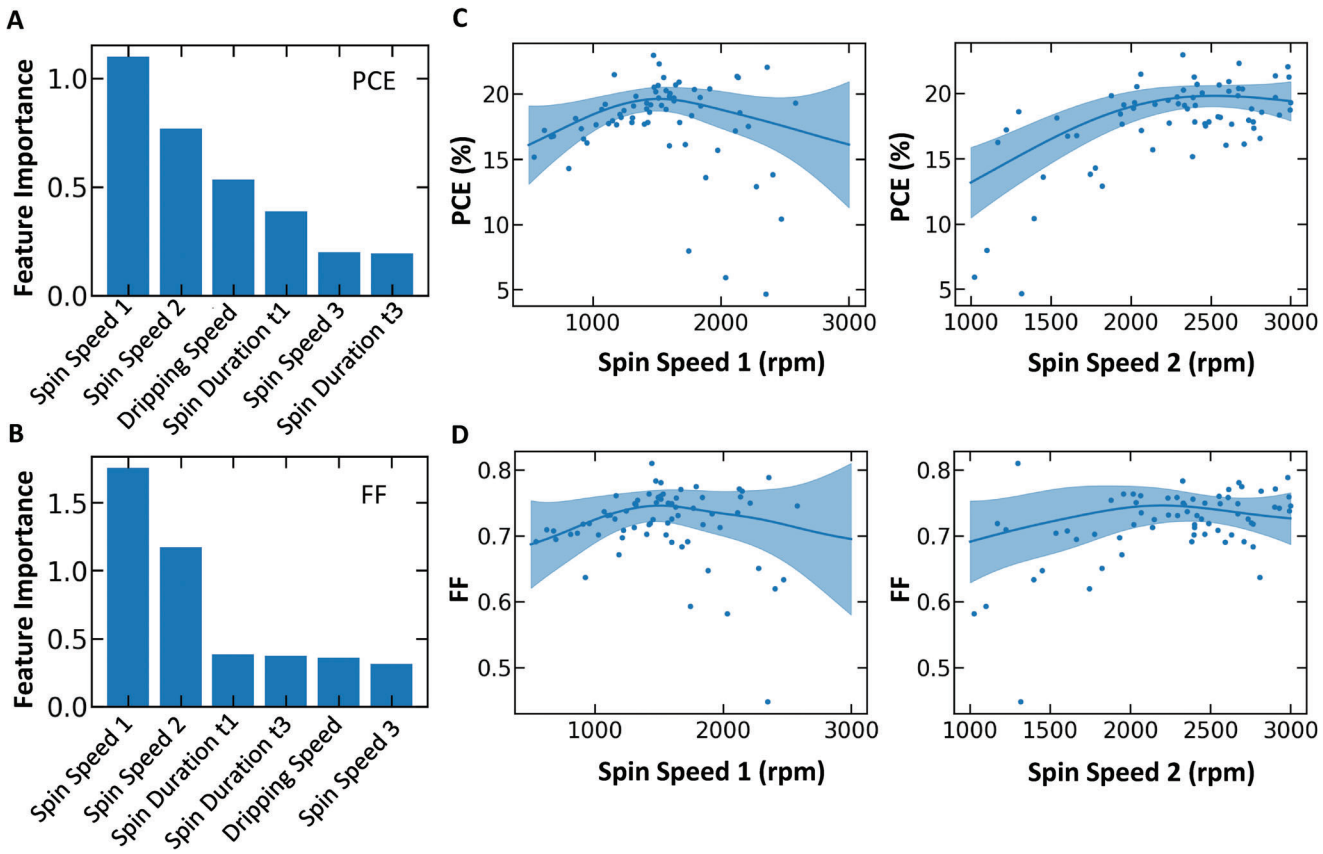

Figure 4. Impact of process parameters on device performance. A) Feature importance of six process parameters influencing the PCE of perovskite devices. B) Feature importance of six process parameters affecting the FF of perovskite devices. C) Scatter plot illustrating the relationship between PCE and spin speeds (spin speed 1 and spin speed 2) during perovskite processing. D) Scatter plot of the relationship between FF and spin speeds (spin speed 1 and spin speed 2) during perovskite processing.

2.4. Results of the Autonomous Optimization

Figure 5 presents the experimental result obtained through the autonomous optimization method. In Figure 5A, the evolution of device efficiency is depicted across iterative optimization rounds. Starting from a complex multidimensional parameter space, the autonomous framework rapidly identified optimal conditions to maximize the perovskite device performance. Out of 77 experimental trials, each trial represents a unique set of process parameters or specific fabrication processes involving six selected variables and several fixed parameters, significant performance improvements were achieved. These results indicate the model's high efficacy in navigating the parameter space and its ability to intelligently select promising conditions without requiring exhaustive testing. During the optimization process, a noticeable hysteresis phenomenon was observed in the *J–V* measurements of devices fabricated in different rounds. This effect, which is commonly seen in regular-structured PSCs, led to differences in efficiency values between forward and reverse scans (see detailed *J–V* curves in Figure S11 in the Supporting Information). To ensure the robustness and practicality of the optimization outcome, the reverse scan results were selected as the primary benchmark for determining device performance. For this optimization process, performance benchmarks were set to classify the resulting devices. Devices with extremely abnormal V_{oc}, J_{sc}, or near-zero efficiency were excluded from the analysis to maintain accuracy (Figure S12, Supporting Information). Devices with an efficiency above 23% were categorized as "good performers," while those achieving a PCE exceeding 23.5% were classified as "top performers." Among the explored parameter sets, five produced "good performers," and notably, one set yielded a "top performer" (**Table 2**). As shown in Figure 5B, the device fabricated using the optimized parameter set achieved a champion PCE of 23.73%, with a V_{oc} of 1.16 V, a J_{sc} of 25.7 mA cm^{-2}, and an FF of 0.79. This outstanding performance is particularly remarkable given that no additives and passivation were used in perovskite processing. In comparison, the reference device fabricated using the conventional OVAT or step-by-step optimization method exhibited a best PCE of 22.0% (Figure 5C). The external quantum efficiency (EQE) spectrum, presented in Figure S13 (Supporting Information), confirms that the integrated current density aligns closely with the values derived from the *J–V* curve, with only a slight deviation. The reproducibility of device performance is evidenced by the *J–V* curves of six cells and repeated experiments (Figure S14, Supporting Information), which show negligible performance variation. This consistency underscores the reliability of the fabrication process and the stability of the device outputs under tested conditions. Figure 5D presents a

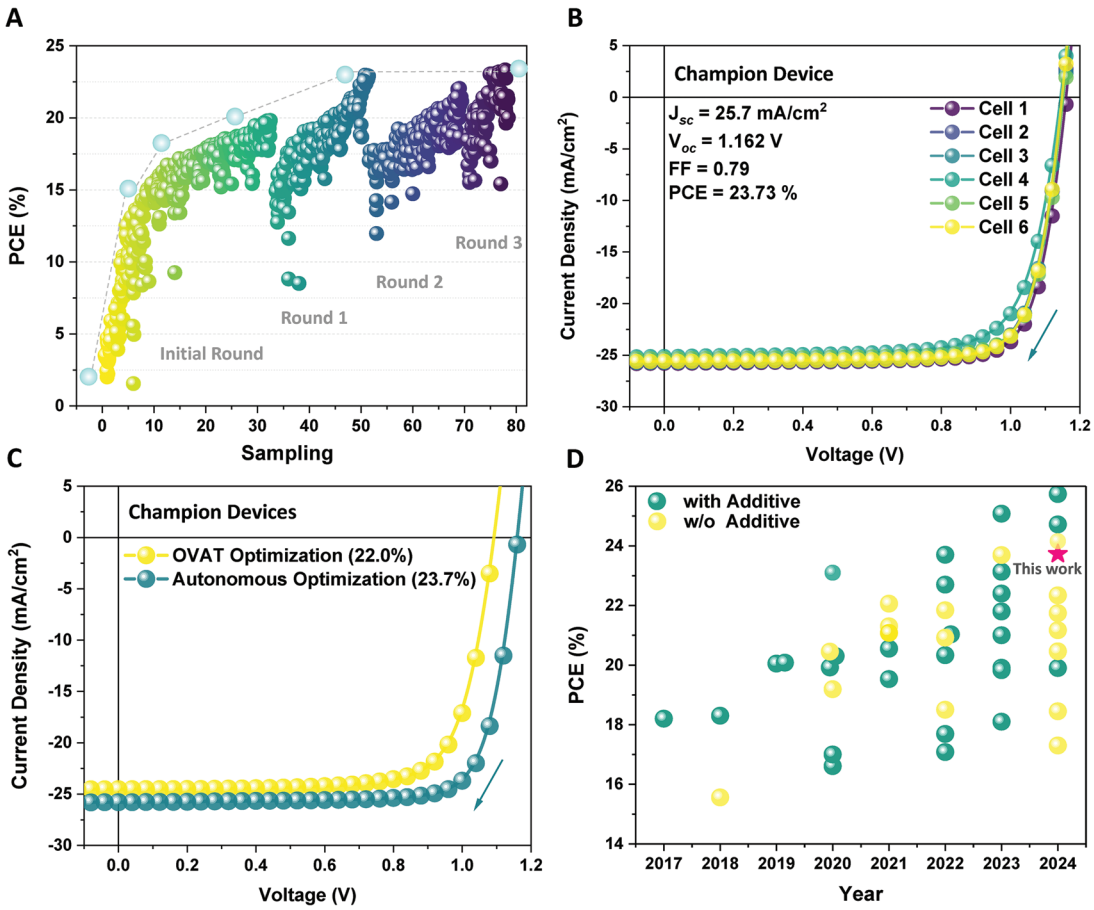

Figure 5. Result of the autonomous optimization experimentation. A) Evolution of device efficiency across three rounds of the iterative optimization process. B) *J–V* curves of the device fabricated using the optimized parameter set. The inset shows the detailed performance metrics. C) Comparison of *J–V* curves for champion cells fabricated under optimized parameters using the OVAT method and the autonomous optimization method. D) Summary of state-of-the-art air-processed perovskite devices fabricated with and without (w/o) additives in the perovskite formulation.

summary of state-of-the-art air-processed perovskite devices with or without additives in the perovskite formulation. Notably, the efficiency achieved in our study ranks among one of the best reported for air-processed PSCs without additives (Table S2, Supporting Information). This achievement highlights the efficacy of the autonomous optimization framework in enhancing PSC performance under ambient conditions.

3. Summary and Outlook

In this study, we introduce an autonomous framework by integrating an automated platform with an ML algorithm to optimize the fabrication process of air-processed perovskite solar cells. Through autonomous exploration of a 6D parameter space, this framework efficiently identified optimal parameter sets within just 77 experimental trials, yielding additive- and passivation-free PSCs with efficiencies of up to 23.7% under ambient conditions. In comparison, the best efficiency achieved using the traditional optimization method was limited to 22.0%. Feature importance analysis revealed that the spin speeds during the first and second steps are critical to device performance and should be prioritized during optimization. These findings demonstrate the superiority of the autonomous framework over traditional methods, which often struggle with exploring multidimensional spaces and are prone to suboptimal local maxima. By reducing dependence on extensive domain-specific knowledge and shifting the focus from local to global optimization, this approach not only improves device performance but also makes the optimization process more resource efficient and accelerates the discovery of optimal manufacturing conditions. Integrating intelligent

Table 2. Process parameter sets for devices classified as "good performers".

Process variable	Spin speed 1 [rpm]	Spin duration t_1 [s]	Spin speed 2 [rpm]	Dripping speed [μL s^{-1}]	Spin duration, t_3 [s]	Spin speed 3 [rpm]
1	925	22	2808	268	5	2000
2	1474	14	2324	250	19	3910
3	1515	16	2676	269	6	3552
4	1165	23	2063	241	32	2863
5	1096	20	2295	247	17	2231

algorithms with automated experimentation demonstrates the transformative potential for rapidly achieving high-performance semiconductor devices and beyond.

Looking ahead, we aim to establish a self-driving Autonomous Material and Device Acceleration Platforms (AMADAP) laboratory.[56,57] This state-of-the-art laboratory, powered by advanced Artificial Intelligence tools, will focus on further advancing the autonomous discovery and development of functional energy materials, pushing the boundaries of intelligent material and device research.

Supporting Information

Supporting Information is available from the Wiley Online Library or from the author.

Acknowledgements

J.Z., J.H., and C.J.B. gratefully acknowledge the grants AutoPeroSol (ZT-I-PF-3-020) and AI-InSu-Pero (ZT-I-PF-5-106) by the Helmholtz Foundation. J.Z. and K.Z. gratefully acknowledge the financial support from the China Scholarship Council (CSC). J.W. gratefully acknowledges financial support from the Sino-German Postdoc Scholarship Program (CSC-DAAD). J.H. and C.J.B. gratefully acknowledge the grants "ELF-PVDesign and development of solution processed functional materials for the next generations of PV technologies" (Grant No. 44-6521a/20/4) by the Bavarian State Government. C.J.B. gratefully acknowledges financial support through the "Aufbruch Bayern" initiative of the state of Bavaria (EnCN and "Solar Factory of the Future") and the German Research Foundation (DFG) SFB 953-No. 182849149 and GRK2495 (ITRG2495).

Open access funding enabled and organized by Projekt DEAL.

Conflict of Interest

The authors declare no conflict of interest.

Author Contributions

J.Z. and C.J.B. conceptualized the research project. J.Z. performed the sample fabrication and characterization experiments. V.M.L.C. and L.L. contributed to the development of the machine learning algorithms. V.M.L.C. and T.O. executed the BO algorithm. J.Z., J.W., and H.Z. analyzed the device data. J.Z. made the figures and wrote the manuscript. J.H. and C.J.B. supervised the project. V.M.L.C., J.W., T.D., and K.Z. assisted in manuscript editing. All authors contributed to the discussion of experimental results and the manuscript.

Data Availability Statement

The data that support the findings of this study are available in the Supporting Information of this article.

Keywords

air-processing perovskite solar cells, automation framework, autonomous optimization, device acceleration platform, machine learning

Received: October 24, 2024
Revised: December 8, 2024
Published online: January 2, 2025

[1] J. Park, J. Kim, H.-S. Yun, M. J. Paik, E. Noh, H. J. Mun, M. G. Kim, T. J. Shin, S. I. Seok, *Nature.* **2023**, *616*, 724.
[2] P. Zhu, D. Wang, Y. Zhang, Z. Liang, J. Li, J. Zeng, J. Zhang, Y. Xu, S. Wu, Z. Liu, X. Zhou, B. Hu, F. He, L. Zhang, X. Pan, X. Wang, N.-G. Park, B. Xu, *Science.* **2024**, *383*, 524.
[3] J. Y. Kim, J.-W. Lee, H. S. Jung, H. Shin, N.-G. Park, *Chem. Rev.* **2020**, *120*, 7867.
[4] Q. Tai, P. You, H. Sang, Z. Liu, C. Hu, H. L. Chan, F. Yan, *Nat. Commun.* **2016**, *7*, 11105.
[5] L. Yan, H. Huang, P. Cui, S. Du, Z. Lan, Y. Yang, S. Qu, X. Wang, Q. Zhang, B. Liu, X. Yue, X. Zhao, Y. Li, H. Li, J. Ji, M. Li, *Nat. Energy.* **2023**, *8*, 1158.
[6] H. Meng, K. Mao, F. Cai, K. Zhang, S. Yuan, T. Li, F. Cao, Z. Su, Z. Zhu, X. Feng, W. Peng, J. Xu, Y. Gao, W. Chen, C. Xiao, X. Wu, M. D. McGehee, J. Xu, *Nat. Energy.* **2024**, *9*, 536.
[7] K. Jung, K. Oh, J. W. Choi, K. C. Kim, M.-J. Lee, *Nano Energy.* **2021**, *89*, 106387.
[8] F. Yang, L. Dong, D. Jang, K. C. Tam, K. Zhang, N. Li, F. Guo, C. Li, C. Arrive, M. Bertrand, *Adv. Energy Mater.* **2020**, *10*, 2001869.
[9] J. Ding, Q. Han, Q.-Q. Ge, D.-J. Xue, J.-Y. Ma, B.-Y. Zhao, Y.-X. Chen, J. Liu, D. B. Mitzi, J.-S. Hu, *Joule.* **2019**, *3*, 402.
[10] Z. Liu, N. Rolston, A. C. Flick, T. W. Colburn, Z. Ren, R. H. Dauskardt, T. Buonassisi, *Joule.* **2022**, *6*, 834.
[11] J. Zhang, B. Liu, Z. Liu, J. Wu, S. Arnold, H. Shi, T. Osterrieder, J. A. Hauch, Z. Wu, J. Luo, J. Wagner, C. G. Berger, T. Stubhan, F. Schmitt, K. Zhang, M. Sytnyk, T. Heumueller, C. M. Sutter-Fella, I. M. Peters, Y. Zhao, C. J. Brabec, *Adv. Energy Mater.* **2023**, *13*, 2302594.
[12] I. M. De Los Santos, H. J. Cortina-Marrero, M. Ruíz-Sánchez, L. Hechavarría-Difur, F. Sánchez-Rodríguez, M. Courel, H. Hu, *Sol. Energy.* **2020**, *199*, 198.
[13] W. Xu, Z. Liu, R. T. Piper, J. W. Hsu, *Sol. Energy Mater. Sol. Cells.* **2023**, *249*, 112055.
[14] A. Raza, K. M. Deen, R. Jaafreh, K. Hamad, A. Haider, W. Haider, *Int. J. Adv. Manuf. Technol.* **2022**, *122*, 1143.
[15] J. George, G. Hautier, *Trends Chem.* **2021**, *3*, 86.
[16] B. Cao, L. A. Adutwum, A. O. Oliynyk, E. J. Luber, B. C. Olsen, A. Mar, J. M. Buriak, *ACS Nano.* **2018**, *12*, 7434.
[17] M. Abolhasani, E. Kumacheva, *Nat. Synth.* **2023**, *2*, 483.
[18] B. P. MacLeod, F. G. Parlane, A. K. Brown, J. E. Hein, C. P. Berlinguette, *Nat. Mater.* **2021**, *21*, 722.
[19] S. Chen, Y. Hou, H. Chen, X. Tang, S. Langner, N. Li, T. Stubhan, I. Levchuk, E. Gu, A. Osvet, *Adv. Energy Mater.* **2018**, *8*, 1701543.
[20] S. Langner, F. Häse, J. D. Perea, T. Stubhan, J. Hauch, L. M. Roch, T. Heumueller, A. Aspuru-Guzik, C. J. Brabec, *Adv. Mater.* **2020**, *32*, 1907801.
[21] X. Du, L. Lüer, T. Heumueller, J. Wagner, C. Berger, T. Osterrieder, J. Wortmann, S. Langner, U. Vongsaysy, M. Bertrand, N. Li, T. Stubhan, J. Hauch, C. J. Brabec, *Joule.* **2021**, *5*, 495.
[22] J. Zhang, S. Langner, J. Wu, C. Kupfer, L. Lüer, W. Meng, B. Zhao, C. Liu, M. Daum, A. Osvet, N. Li, M. Halik, T. Stubhan, Y. Zhao, J. A. Hauch, C. J. Brabec, *ACS Energy Lett.* **2022**, *7*, 70.
[23] Y. Shang, Z. Xiong, K. An, J. A. Hauch, C. J. Brabec, N. Li, *MGE Adv.* **2024**, *2*, e28.
[24] Y. Zhao, T. Heumueller, J. Zhang, J. Luo, O. Kasian, S. Langner, C. Kupfer, B. Liu, Y. Zhong, J. Elia, A. Osvet, J. Wu, C. Liu, Z. Wan, C. Jia, N. Li, J. Hauch, C. J. Brabec, *Nat. Energy.* **2022**, *7*, 144.
[25] J. Wu, J. Zhang, M. Hu, P. Reiser, L. Torresi, P. Friederich, L. Lahn, O. Kasian, D. M. Guldi, M. E. Pérez-Ojeda, A. Barabash, J. S. Rocha-Ortiz, Y. Zhao, Z. Xie, J. Luo, Y. Wang, S. I. Seok, J. A. Hauch, C. J. Brabec, *J. Am. Chem. Soc.* **2023**, *145*, 16517.
[26] T. C. Wu, A. Aguilar-Granda, K. Hotta, S. A. Yazdani, R. Pollice, J. Vestfrid, H. Hao, C. Lavigne, M. Seifrid, N. Angello, F. Bencheikh, J.

E. Hein, M. Burke, C. Adachi, A. Aspuru-Guzik, *Adv. Mater.* **2023**, *35*, 2207070.
[27] M. M. Flores-Leonar, L. M. Mejía-Mendoza, A. Aguilar-Granda, B. Sanchez-Lengeling, H. Tribukait, C. Amador-Bedolla, A. Aspuru-Guzik, *Curr. Opin. Green Sustainable Chem.* **2020**, *25*, 100370.
[28] P. M. Attia, A. Grover, N. Jin, K. A. Severson, T. M. Markov, Y.-H. Liao, M. H. Chen, B. Cheong, N. Perkins, Z. Yang, *Nature.* **2020**, *578*, 397.
[29] D. P. Tabor, L. M. Roch, S. K. Saikin, C. Kreisbeck, D. Sheberla, J. H. Montoya, S. Dwaraknath, M. Aykol, C. Ortiz, H. Tribukait, C. Amador-Bedolla, C. J. Brabec, B. Maruyama, K. A. Persson, A. Aspuru-Guzik, *Nat. Rev. Mater.* **2018**, *3*, 5.
[30] J. Zhang, J. Wu, S. Langner, B. Zhao, Z. Xie, J. A. Hauch, H. A. Afify, A. Barabash, J. Luo, M. Sytnyk, W. Meng, K. Zhang, C. Liu, A. Osvet, N. Li, M. Halik, W. Heiss, Y. Zhao, C. J. Brabec, *Adv. Funct. Mater.* **2022**, *32*, 2207101.
[31] J. Zhang, J. Wu, Y. Zhao, Y. Zou, A. Barabash, Z. Wu, K. Zhang, C. Deng, J. Elia, C. Li, J. S. Rocha-Ortiz, C. Liu, A. Saboor, I. M. Peters, J. A. Hauch, C. J. Brabec, *ACS Energy Lett.* **2023**, *8*, 3595.
[32] S. Sun, N. T. Hartono, Z. D. Ren, F. Oviedo, A. M. Buscemi, M. Layurova, D. X. Chen, T. Ogunfunmi, J. Thapa, S. Ramasamy, *Joule.* **2019**, *3*, 1437.
[33] J. Yang, B. J. Lawrie, S. V. Kalinin, M. Ahmadi, *Adv. Energy Mater.* **2023**, *13*, 2302337.
[34] Y. Zhao, J. Zhang, Z. Xu, S. Sun, S. Langner, N. T. P. Hartono, T. Heumueller, Y. Hou, J. Elia, N. Li, G. J. Matt, X. Du, W. Meng, A. Osvet, K. Zhang, T. Stubhan, Y. Feng, J. Hauch, E. H. Sargent, T. Buonassisi, C. J. Brabec, *Nat. Commun.* **2021**, *12*, 2191.
[35] N. Meftahi, M. A. Surmiak, S. O. Fürer, K. J. Rietwyk, J. Lu, S. R. Raga, C. Evans, M. Michalska, H. Deng, D. P. McMeekin, *Adv. Energy Mater.* **2023**, *13*, 2203859.
[36] B. Burger, P. M. Maffettone, V. V. Gusev, C. M. Aitchison, Y. Bai, X. Wang, X. Li, B. M. Alston, B. Li, R. Clowes, N. Rankin, B. Harris, R. S. Sprick, A. I. Cooper, *Nature.* **2020**, *583*, 237.
[37] A. E. Gongora, B. Xu, W. Perry, C. Okoye, P. Riley, K. G. Reyes, E. F. Morgan, K. A. Brown, *Sci. Adv.* **2020**, *6*, eaaz1708.
[38] S. Lu, Q. Zhou, Y. Ouyang, Y. Guo, Q. Li, J. Wang, *Nat. Commun.* **2018**, *9*, 3405.
[39] K. Higgins, S. M. Valleti, M. Ziatdinov, S. V. Kalinin, M. Ahmadi, *ACS Energy Lett.* **2020**, *5*, 3426.
[40] Q. Liang, A. E. Gongora, Z. Ren, A. Tiihonen, Z. Liu, S. Sun, J. R. Deneault, D. Bash, F. Mekki-Berrada, S. A. Khan, K. Hippalgaonkar, B. Maruyama, K. A. Brown, J. Fisher Iii, T. Buonassisi, *npj Comput. Mater.* **2021**, *7*, 188.
[41] A. G. Kusne, H. Yu, C. Wu, H. Zhang, J. Hattrick-Simpers, B. DeCost, S. Sarker, C. Oses, C. Toher, S. Curtarolo, *Nat. Commun.* **2020**, *11*, 5966.
[42] B. P. MacLeod, F. G. L. Parlane, T. D. Morrissey, F. Häse, L. M. Roch, K. E. Dettelbach, R. Moreira, L. P. E. Yunker, M. B. Rooney, J. R. Deeth, V. Lai, G. J. Ng, H. Situ, R. H. Zhang, M. S. Elliott, T. H. Haley, D. J. Dvorak, A. Aspuru-Guzik, J. E. Hein, C. P. Berlinguette, *Sci. Adv.* **2020**, *6*, eaaz8867.
[43] T. Osterrieder, F. Schmitt, L. Lüer, J. Wagner, T. Heumüller, J. Hauch, C. J. Brabec, *Energy Environ. Sci.* **2023**, *16*, 3984.
[44] J. Zhang, J. Wu, A. Barabash, T. Du, S. Qiu, V. M. Le Corre, Y. Zhao, K. Zhang, F. Schmitt, Z. Peng, J. Tian, C. Li, C. Liu, T. Heumueller, L. Lüer, J. A. Hauch, C. J. Brabec, *Energy Environ. Sci.* **2024**, *17*, 5490.
[45] J. Wagner, C. G. Berger, X. Du, T. Stubhan, J. A. Hauch, C. J. Brabec, *J. Mater. Sci.* **2021**, *56*, 16422.
[46] https://github.com/i-MEET/boar (accessed: May 2024).
[47] C. Kupfer, V. M. Le Corre, C. Li, L. Lüer, K. Forberich, M. Kato, A. Osvet, C. J. Brabec, *J. Mater. Chem. C.* **2024**, *12*, 95.
[48] M. Wagner, A. Distler, V. M. Le Corre, S. Zapf, B. Baydar, H.-D. Schmidt, M. Heyder, K. Forberich, L. Lüer, C. J. Brabec, H. J. Egelhaaf, *Energy Environ. Sci.* **2023**, *16*, 5454.
[49] M. Balandat, B. Karrer, D. Jiang, S. Daulton, B. Letham, A. G. Wilson, E. Bakshy, *Adv. Neural Inf. Process. Syst.* **2020**, *33*, 21524.
[50] https://github.com/facebook/Ax (accessed: May 2024).
[51] https://zenodo.org/records/1207017 (accessed: May 2024).
[52] D. Eriksson, M. Jankowiak, presented at Uncertainty in Artificial Intelligence, **2021**, *161*, 493. https://proceedings.mlr.press/v161/eriksson21a.html
[53] https://ax.dev/tutorials/saasbo.html. (May, 2024)
[54] Q. Jiang, Z. Chu, P. Wang, X. Yang, H. Liu, Y. Wang, Z. Yin, J. Wu, X. Zhang, J. You, *Adv. Mater.* **2017**, *29*, 1703852.
[55] Q. Song, Y. Bai, Q. Chen, *J. Phys. Chem. Lett.* **2022**, *13*, 10741.
[56] J. Zhang, J. A. Hauch, C. J. Brabec, *Acc. Chem. Res.* **2024**, *57*, 1434.
[57] J. Zhang, J. Wu, O. Stroyuk, O. Raievska, L. Lüer, J. A. Hauch, C. J. Brabec, *MRS Bulletin.* **2024**, *49*, 1284.